Can microscale fracture tests provide reliable fracture toughness values? A case study in silicon

Balila Nagamani Jaya
Structure and Nano/Micro-mechanics of Materials, Max-Planck-Institut für Eisenforschung GmbH, Düsseldorf 40237, Germany

Christoph Kirchlechner
Structure and Nano/Micro-mechanics of Materials, Max-Planck-Institut für Eisenforschung GmbH, Düsseldorf 40237, Germany; and University of Leoben, Leoben 8700, Austria

Gerhard Dehm[a)]
Structure and Nano/Micro-mechanics of Materials, Max-Planck-Institut für Eisenforschung GmbH, Düsseldorf 40237, Germany

(Received 2 October 2014; accepted 17 December 2014)

Fracture toughness testing of materials at the micrometer scale has become essential due to the continuing miniaturization of devices accompanied by findings of size effects in fracture behavior. Many techniques have emerged in the recent past to carry out fracture toughness measurements at the relevant micro and nanolength scales, but they lack ASTM standards that are prescribed for bulk scale tests. Also, differences in reported values arise at the microscale due to the sample preparation technique, test method, geometry, and investigator. To correct for such discrepancies, we chose four different fracture toughness test geometries in practice, all of them micromachined in the focused ion beam (FIB), to investigate the fracture toughness of Si(100) at the micrometer scale. The average K_{IC} that emerges from all four cases is a constant (0.8 MPa $m^{1/2}$). The advantages and limitations of each of these geometries in terms of test parameters and the range of materials that can be tested are discussed.

I. INTRODUCTION

Device miniaturization and shrinking internal material length scales have pushed the mechanics community to investigate deformation and fracture behavior of materials at ever smaller length scales. The principal problem that crops up with reducing sample dimensions is that size effects cannot be accounted for by direct extrapolation of known properties at the macroscale. Two of the most widely known size effects pertaining to strength of materials deal with the extrinsic (smaller is stronger)[1–3] and intrinsic (Hall–Petch like effects)[4,5] material length scales, respectively. Although known as a characteristic material property, many reports on K_{IC} for the same given materials show variations due to the geometry, sample dimensions, and preparation techniques. One example is that of pure single crystal silicon, Si(100), a homogeneous, and ideally elastic–brittle material. The reported K_{IC} as found from tension, bending, and indentation experiments both at the bulk and small-scales for Si(100) shows a wide scatter, anywhere from 0.7 to 2.1 MPa $m^{1/2}$.[6–10] The largely agreed value though is between 0.7 and 1.3 MPa $m^{1/2}$ for single crystal Si.[11] One of the reasons for this scatter in reported values could be due to the inability at small length scales to strictly adhere to the ASTM standards, which prescribe exact sample dimensions and crack sizes for a valid fracture toughness test.[12] As the sample dimensions become smaller, the relative plastic zone size becomes larger and hence maintaining plane strain and linear elastic fracture mechanics (LEFM) conditions becomes difficult, which in turn bring in the controversy as to whether the observed size effect is real or apparent. To avoid underestimation of fracture toughness and unsubstantiated safety factors, the material is tested best at the scale at which it is used in real application. Also in some cases, the amount of material available is scarce, in which case one is forced to determine fracture properties within the available small volume. Moreover, bulk scale testing can lead to loss of information, especially in materials showing stable crack growth and *R*-curve behavior, due to overload or during fatigue precracking of such specimen.

The development of instruments to both apply and measure loads and displacements accurately as well as to observe the deformation as it proceeds in situ at smaller dimensions has enabled fracture toughness testing of materials at micrometer and nanometer sizes to become

Contributing Editor: George M. Pharr
[a)]Address all correspondence to this author.
e-mail: dehm@mpie.de
DOI: 10.1557/jmr.2015.2

 © Materials Research Society 2015

https://doi.org/10.1557/jmr.2015.2 Published online by Cambridge University Press

a reality.[13] Simultaneously, there has been a spurt in the availability of micromachining techniques like focused ion beam (FIB) machining, lithography, deep reactive ion etching (DRIE), and laser machining to prepare samples at ever smaller dimensions.[14] Specially equipped scanning electron microscopes (SEM) are being used today as microlaboratories, replacing bulk tests.[15,16] Testing in situ inside the SEM enables using smaller specimens but on the flip side, smaller sample sizes make it difficult to maintain LEFM and plane strain conditions in materials with significant plasticity. Also an expanding process zone in a material with a rising *R*-curve cannot be captured beyond a critical crack length (*a*)/specimen width (*w*) ratio, since the crack begins to "see" the free surface after a point.[17] Information on the processes within the interior of the material is lost, since SEM imaging gives only surface information. This causes a problem in observing the actual toughening mechanisms operating in the material. In spite of these general limitations for in situ fracture toughness tests inside the SEM, there are several advantages that such instruments provide to probe small volumes. In situ testing allows simultaneous and synchronous recording of the load–displacement information and crack initiation and propagation events. This enables fracture loads to be precisely noted, as also accurate determination of crack opening displacements (COD) via direct observation or by digital image correlation (DIC), important in fracture mechanics experiments at the small-scale. For materials exhibiting a rising fracture toughness (*R*-curve), in situ imaging allows one to capture the crack trajectory during different stages of crack growth under both static and cyclic loads, enabling determination of the fracture and fatigue mechanisms at the small-length scale.[17] The same does not apply to brittle systems exhibiting very high crack propagation velocities and catastrophic failure though. But sufficient care needs to be exercised in separating out the actual material displacements from that due to the instrument, even in sufficiently stiff machines, because smaller loads and displacements are involved.[18] This is especially important in material systems where stable crack growth is hard to achieve. The loading system is expected to have a frame stiffness much higher (by 2–3 orders of magnitude) than the material being tested but this may not always be the case at smaller dimensions. For instance, commercial nanoindenters used inside the SEM for in situ measurements have a high load frame compliance (over 10 nm/mN[19–21]), which is at least an order of magnitude higher than conventional universal testing machines (0.16 nm/mN[22]). This prevents a stiff enough machine required to achieve true fixed-grip conditions. Although, using nanoindenters is better than using AFM or micromanipulators with an even higher compliance, the fraction of the energy that is stored in the load frame is still a large part of the total energy expended in carrying out tests at the small scale. Displacement control is a prerequisite for stable crack growth under most geometries. The presently available indenter systems are often intrinsically load controlled but provide for depth control via a feedback loop from the displacement sensor. The frequency of this feedback channel (~80 kHz for the Hysitron PI series) is sufficient to provide true depth control for routine indentation tests, but falls short of matching the velocity of crack propagation. The depth change during the associated pop-in in the load (*P*)–displacement (*d*) curve is much more rapid and hence difficult to control.[23] Therefore, accurate *R*-curve measurements in such systems may be difficult to perform. The ASMEC UNAT-2 setup used in the present work is intrinsically displacement controlled using highly compliant springs (>1000 nm/mN), which adds versatility to the type of tests that can be carried out but hinders controlled crack propagation in fracture studies. Peret and Rodrigues[24] elaborate on the importance of machine stiffness in attaining stable crack propagation in displacement controlled three point bend tests, highlighting the effect of the stored elastic energy in some of the low stiffness machine parts. The release of this energy during crack propagation will result in instabilities and increase speed of propagation.

Given the discrepancies that exist in reported values of K_{IC} of Si in the literature, the effect of four different microscale testing geometries (Fig. 1) on the fracture toughness of single crystal Si(100) was probed in the present work. Instead of round robin tests that are carried out between different groups to establish material properties objectively, we applied different test methods to analyze whether differences arise in the deduced fracture toughness values. Extraneous effects that arise due to change in the investigator, sample dimensions, and purity were eliminated by restricting all the tests to one single Si(100) wafer, micromachined by the FIB to similar beam dimensions on an average and loaded using an indenter in situ inside the SEM. Since the plastic zone size of Si is not larger than 0.25 μm (with a conservative estimate assuming a K_{IC} of 0.75 MPa $m^{1/2}$ and a yield stress σ_y of 500 MPa[11]), the sample dimensions chosen here adhere to LEFM and plane strain conditions. K_{IC} as determined from all the four chosen geometries is reported along with a discussion on the advantages and limitations of each of them. None of them are typical scaled down versions of bulk test geometries but show some resemblance to the macroscopic cases with several modifications. The choice of these four geometries was made because they are relatively new and specifically used in small-scale testing. Being nonstandard geometries, it is important to compare the K_{IC}'s obtained from them in a single given material with known fracture toughness, which has not been done before. Pure, single crystal Si in a

https://doi.org/10.1557/jmr.2015.2 Published online by Cambridge University Press

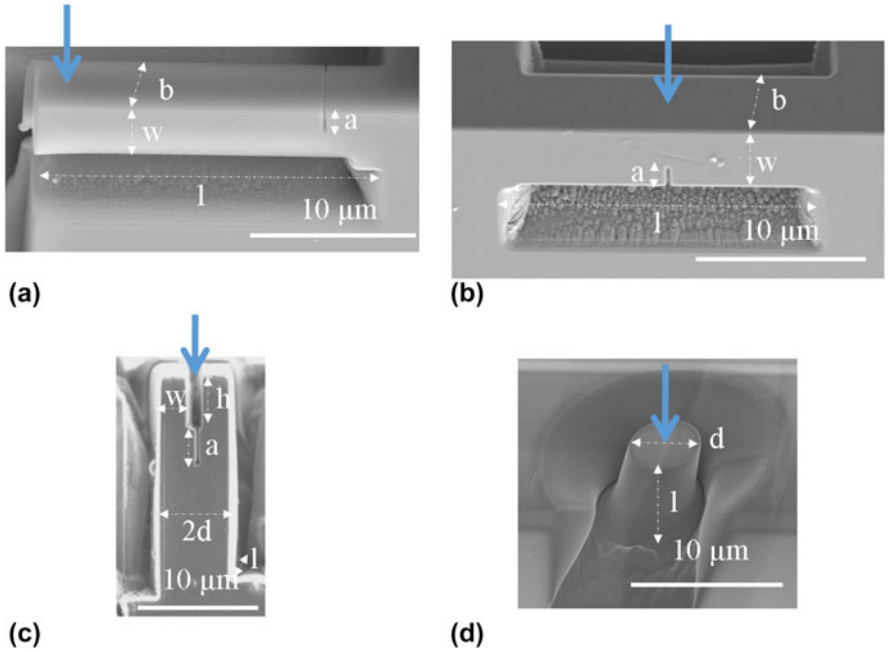


FIG. 1. Four different geometries selected for fracture toughness testing at the small scale: (a) single cantilever bending, (b) clamped beam bending, (c) DCB, and (d) pillar splitting. All samples were machined and notched using the FIB on a straight edge of Si(100).

given orientation was chosen to avoid effects of interfaces and alloying additions on a property like fracture toughness which is known to be very sensitive to the above factors. Also, it was ensured that the initial notching and loading direction drive the crack in the same plane and direction in all the four cases. A discussion on the more general aspects affecting small-scale fracture toughness testing, like effect of FIB milling, finite value of notch root radius, sample dimensions compared to the plastic zone size, follows. A guideline for future users highlighting the usefulness of each geometry and possible sources of error is given in the end.

TABLE I. Fracture toughness of Si(100) as obtained from five valid tests in each geometry. The sample dimensions mentioned above are average values, with individual differences being attributed to minor shifts during FIB milling.

Geometry	Sample dimensions (μm)	Crack length "a" (μm)	K_{IC} (MPa $m^{1/2}$)
1. Single cantilever bend	20 × 5 × 5	2.3	0.76 ± 0.08
2. Clamped bean bend	20 × 5 × 5 and 40 × 5 × 5	2	0.81 ± 0.10
3. Double cantilever compression	4 × 2 × 2	2	0.89 ± 0.12
4. Pillar splitting	5 × 8.5	...	0.75 ± 0.16

II. EXPERIMENTAL PROCEDURE

A Si(100) wafer was scratched by a diamond scribe and sliced to get a straight edge and mounted in the FIB (Zeiss AURIGA, Germany) for micromachining. Four different geometries were chosen from the literature for fracture toughness testing: (1) single cantilever bending[25] with 5 μm conical indenter tip; (2) clamped beam bending[26] with 5 μm conical tip; (3) double cantilever bending (DCB) with 5 μm flat punch indenter tip[27]; and (4) pillar splitting[28] with cube corner indenter tip. Five samples were tested for each type. The custom-made indenter tips, made of B-doped diamond, were supplied by ASMEC GmbH (Germany). The governing dimension was in the range of few micrometers for all the sample geometries, as listed in Table I. This ensured that the LEFM and plane strain criteria were satisfied for Si. The test geometries with their exact dimensions and nomenclature used to describe them are shown in Fig. 1. Notches were milled at lower currents to act as starter cracks along (010)<001>. All the microbeams were milled at the straight edge using the following conditions: (a) 30 kV, 4 nA aperture for coarse cuts, (b) 30 kV, 600 pA aperture for final polishing and removal of redeposited material, and (c) 30 kV, 10 pA aperture for notching. Ga^+ ion damage was minimized by viewing the milling process using the secondary electron (SE) imaging of the electron microscope. The sample was then loaded in a nanoindenter (ASMEC UNAT SEM-2) inside the SEM for direct viewing of the fracture process while simultaneously recording the load (P)–displacement (d) information. All the loading was carried out in open loop displacement control at ~5 nm/s. Since the point of onset of contact was to be

https://doi.org/10.1557/jmr.2015.2 Published online by Cambridge University Press

accurately determined for measurement of fracture loads, the indentation programme was setup such that the *P–d* curve was recorded while the indenter tip began to approach the surface from a distance about 500 nm away from the sample. This distance could be maintained accurately using the real-time SEM imaging. The point of onset of contact was defined as the point in the *P–d* curve when there was a transition from zero load to a finite load (which showed up as a spike in stiffness). This portion of the curve showing zero load was later subtracted. Cyclic load–unload was carried out with sufficient hold times to record every stage of crack growth. Crack propagation was detected as a pop-in the *P–d* curve and the exact crack length was measured by extracting the corresponding snapshots of the SEM images from the recorded video. Crack opening displacement was not measured in the present work since LEFM calculations suffice for Si, an ideally elastic brittle system, but it is of relevance to systems which exhibit significant crack tip plasticity. Such materials may also not display a clear pop-in but instead show gradual drop in stiffness of the *P–d* curve.[17] The fracture load corresponding to the crack propagation event was used as input in available analytical solutions[25,27,28] for geometries 1, 3, and 4, respectively or in finite element method (FEM) simulated K_I versus P curves (as carried out in ABAQUS 6.12 for geometry 2)[29] to extract the K_{IC}. The simulation procedure for the clamped beam geometry was explained already in detail[26] and will not be repeated here. The elastic modulus of Si(100) was taken to be 169 GPa as per the guidelines given for monocrystalline anisotropic Si.[30]

Specifications for a valid test for each individual geometry are given below:

A. Single cantilever bending

Beam dimensions should adhere to a *l*/*w* ratio greater than 4 and an initial *a*/*w* ratio ideally between 0.45 to 0.55.[25] The indenter position should be close to the free end at a minimum distance of four times the width of the beam from the initial notch, to minimize the shear component of loading.[31] Large cantilever deformations can be accompanied by slipping of the indenter on the beam surface when the indenter does not possess sufficient lateral stiffness. Slipping shows up in the *P–d* curve as random displacement jumps not associated with any crack propagation. This can be avoided to an extent by using sharp indenters (which is mostly the case as seen from the literature[27]) but in such cases the indentation contribution to the total displacement has to be accounted for. In the other case, where a blunt wedge/conical tip is used, like in the present work, in situ imaging helps to correlate pop-in in the *P–d* curve to real crack propagation events. In the present work, no such slipping was observed. Elastic deformation must be ensured by cyclically loading and unloading below the expected fracture load a couple of times to check for any remnant displacement in the *P–d* curve. K_I is given by Eq. (1a) (Ref. 25) and requires precise knowledge of beam dimensions, fracture load, and elastic modulus of the specimen material in the given orientation. This formula cannot be used if the crack deviates from its straight path and kinks at an angle instead, since this will violate mode I loading conditions.

$$K_I = \frac{P_{max} l}{b w^{3/2}} f\left(\frac{a}{w}\right) \quad , \tag{1a}$$

$$f\left(\frac{a}{w}\right) = 1.46 + 24.36\left(\frac{a}{w}\right) - 47.21\left(\frac{a}{w}\right)^2 + 75.18\left(\frac{a}{w}\right)^3 \quad , \tag{1b}$$

where P_{max} is the fracture load, l, b, and w refer to beam dimensions, and a is the crack length as shown in Fig. 1(a). $f(a/w)$ is the geometric factor[25] given by Eq. (1b).

B. Clamped beam bending

Beam dimensions should adhere to a *l*/*w* ratio between 4 and 8 and an initial *a*/*w* ratio between 0.3 and 0.5. A much shorter or longer starting crack length will not provide stable crack growth and also give rise to free surface effects.[29] The maximum principal stress that opens up the crack acts along the line connecting the notch tip and the indenter. Therefore, the indenter should ideally be positioned exactly across the notch for mode I loading but misalignments up to 5% of beam length are tolerable. The indenter tip should be sufficiently blunt to not cause indentation impressions or cracking. The test is no more valid if and when edge cracking initiates at the clamped ends. Maintaining larger *l*/*w* ratios prevents edge cracking. K_I is obtained via extended finite element method (XFEM) simulations and has a sinusoidal dependence on *a*/*w*.[29] This is unlike the monotonic increase in K_I that is seen as a function of *a*/*w* in other geometries. Though the general form of this dependence remains constant for this geometry, each case differing in sample dimensions has to be separately simulated for quantitative determination of K_I in the absence of readily available analytical solutions.

C. Double cantilever bending

Beam dimensions should adhere to $w = d/2$ and $(h + a) > 4w$. Symmetry plays an important role in this geometry. The two arms should be of equal width (w). The flat punch indenter surface must be exactly parallel to the two cantilever heads to make contact with both the arms simultaneously. This ensures mode I loading. The flat punch width should ideally be larger than the total width of

https://doi.org/10.1557/jmr.2015.2 Published online by Cambridge University Press

the two cantilevers (2d) together. K_I is given by Eq. (2) (Ref. 27) and requires knowledge of the coefficient of friction μ between the diamond tip and sample. The test is not valid if the crack kinks away from the straight path or fracture initiates elsewhere (e.g., in the cantilever arms). It is also not valid if plasticity results due to compression of the cantilevers which in turn requires that a certain condition is imposed on the total sample width depending on its K_{IC}/σ_y ratio as shown by Liu et al.[27]

$$K_I = \sqrt{3}\frac{(e - \mu h)}{bd^3/2}P_{max} \quad , \qquad (2)$$

where P_{max} is the fracture load and $e = (d - w)/2$. d, w, b, and h are beam dimensions as shown in Fig. 1(c).

D. Pillar splitting

Beam dimensions should adhere to an l/d ratio close to 1. Longer beams will give rise to buckling which renders the test invalid. This is the only geometry which does not require a notched sample. The indenter tip has to be positioned roughly at the center of the pillar, though minor misalignments will not affect the K_{IC} measurement adversely. This positioning requires a viewing window from the top of the pillar, which is possible only if the indenter is titled by an angle with respect to the electron beam in an in situ test. K_I is obtained using Eq. (3) (Ref. 28), which is independent of crack length and requires accurate knowledge of the E/H ratio and Poisson's ratio ν of the material and friction coefficient μ between the tip and the sample. The value of γ that appears in Eq. (3) is material specific and needs to be determined via FEM simulations using the cohesive zone model for each individual case and indenter geometry. As of now, these calculations are possible for a host of E/H ratios but only for isotropic, homogeneous materials indented by a Berkovich.[28] The energy for fracture in this geometry includes both crack initiation and propagation events, unlike other geometries which are prenotched. The effect of crack length (which is generated during indentation) and its relation to the pillar radius is not yet clear, but for a valid test, it has to be ensured that the edge cracking that initiates under the indenter tip should reach the pillar wall and split it open into three parts. If the cracking is restricted to within the pillar, this will resemble a typical indentation fracture toughness test on which Eq. (3) cannot be used.

$$K_c = \frac{\gamma P_{max}}{R^3/2} \quad , \qquad (3)$$

where P_{max} is the fracture load, γ is the FEM simulated dimensionless constant for the given E/H ratio, and R is the pillar radius given by $d/2$, as shown in Fig. 1(d). A γ value of 0.305 was determined from FEM simulations by Sebastiani[32] for an $E/H = 14.3$ (Ref. 33) for Si(100). From the data available in Sebastiani, γ is seen to decrease with decreasing E/H ratio and is extremely sensitive to this ratio, while showing independence with respect to the aspect ratio of the pillar. A lower γ would be inference means higher fracture loads for a given fracture toughness and pillar radius of the material.

III. RESULTS AND DISCUSSION

The samples before and after fracture along with the load–displacement curves are shown in Fig. 2. Si(100) is a single crystal and hence expected to show anisotropy in properties. Hence, it was ensured that the notch was held constant along (010) in all the test geometries requiring a precrack [Figs. 2(a)–2(c)]. Also, the P–d curves shown in Fig. 2-III(a,d) reinforce the fact that Si deforms in an ideally elastic–brittle fashion. Like for all microscale tests, the need to have a good load/displacement resolution as well as accurate determination of sample dimensions cannot be stressed enough. The minor differences seen in the average fracture toughness values obtained from individual geometries can be attributed to the difference in the stress state that each of them experience. The K_{IC} results and advantages and limitations of each of the four geometries are reported and discussed below:

A. Single cantilever bending

Single cantilever bending [Fig. 2(a)] is the most common fracture toughness test geometry that has been used at the small-scale till date.[25,34–38] Although the use of rectangular beams and straight cut notches has been the most commonly used, due to the straightforward analytical solutions for K_I available for the same, there are instances of pentagonal or trigonal shaped beams,[39,41] with bridge[25] or chevron[40] notches also being tested, using finite element solutions for K_I. The bridge and chevron notches initiate real cracks in the system on loading and hence avoid "notch effects". Notches can be machined both from the side and from the top,[41] which gives more degrees of freedom in positioning along particular features of the microstructure. Though this geometry is not very commonly used in bulk cases, it is easy and simple to both micromachine and perform fracture experiments in such specimens. The advantage of this geometry lies in its ability to test a range of materials, boundaries, and interfaces, since such beams can be machined at any location with great ease, although restricted to the elastic–brittle regime. Though it is difficult to achieve pure mode I loading conditions due to asymmetric nature of bending of such a beam, the shear component can be minimized by increasing the l/w ratio (>4).[31] But longer beams mean more FIB

https://doi.org/10.1557/jmr.2015.2 Published online by Cambridge University Press

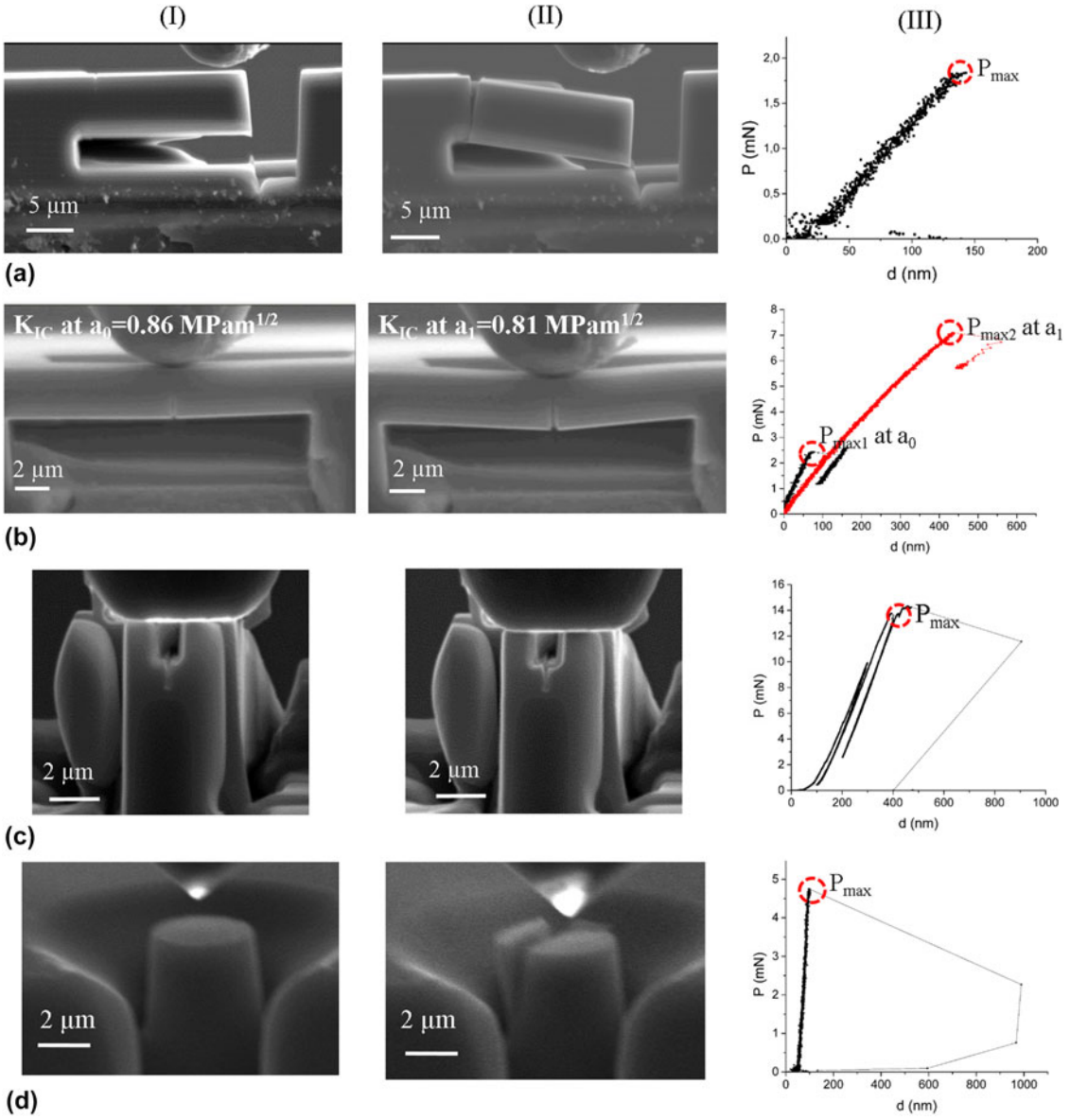


FIG. 2. Snapshots of the samples (I) before and (II) after fracture and (III) the corresponding *P–d* curve. (a–d) refer to the four geometries used for fracture toughness testing.

machining time and higher probability of the indenter sliding away as the beam deforms to larger displacements before failure. Also, this geometry is inherently unstable and crack growth is catastrophic in materials which do not show any *R*-curve. Therefore, one can only obtain the initiation fracture toughness from such tests. The fracture surface at the fixed end is clearly visible and can be used for post-examination studies due to the fracture running across the entire beam width, although the test beams cannot be retained after failure for the same reason. K_I [see Eq. (1)] is very sensitive to an accurate measurement of the beam dimensions and the distance between the loading point and the precrack which is why in situ imaging becomes indispensable for this geometry.

For Si(100), a K_{IC} of 0.76 ± 0.08 was found from this geometry.

B. Clamped beam bending

Clamped beam bending [Fig. 2(b)] was first demonstrated as a fracture test geometry recently on PtNiAl bond coats.[26] Based on a modification over the classical three point bend test by clamping the ends instead of letting them free, this geometry offers pure mode I loading as well as controlled mixed mode loading by placing the indenter at fixed offsets from the notch position. The key advantage of this geometry over the single cantilever though is its ability to support stable crack growth, even in brittle systems with no *R*-curve.

https://doi.org/10.1557/jmr.2015.2 Published online by Cambridge University Press

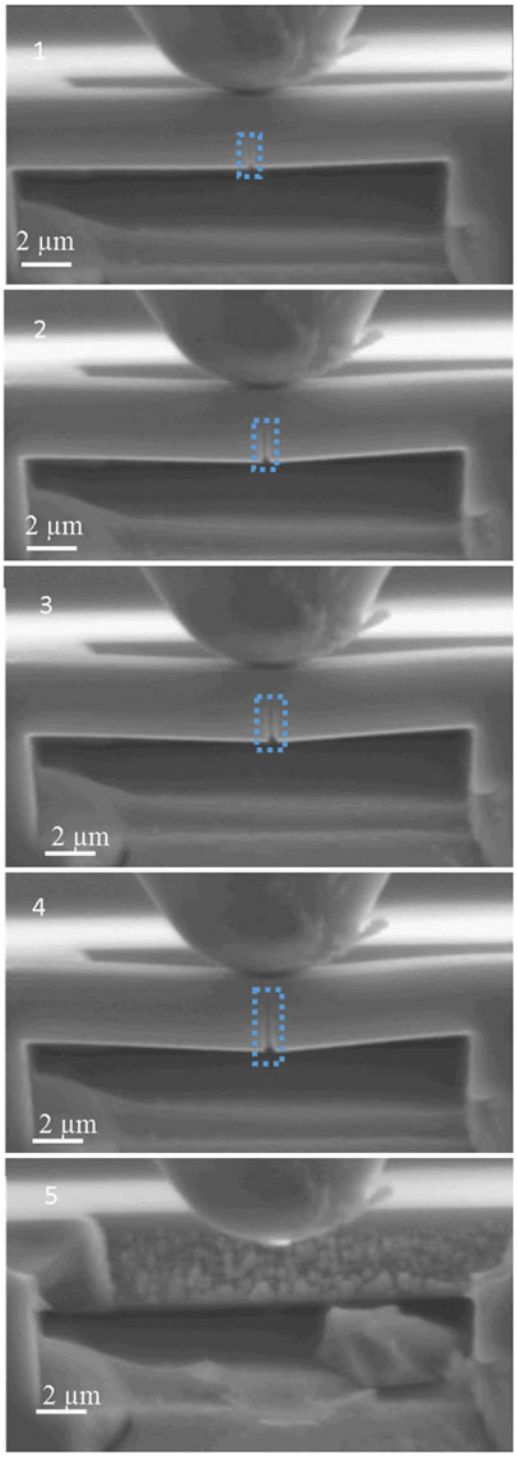


FIG. 3. Various stages (1–5) of crack growth and arrest (see dotted rectangles in blue) in a Si(100) clamped beam, before complete failure ensues, showing stability of the geometry.

This can be seen more clearly from Fig. 3 where the crack is seen to grow and arrest in stages before complete failure ensues. The associated *P–d* curve [Fig. 2(b-III)] shows the first pop-in load at the first crack propagation event, and the next one at a higher load when the beam finally fractures completely. The reduced slope in the second loading cycle accounts for the decreased stiffness of the beam now containing a longer crack. Such controlled crack growth is important in the measurements of *R*-curve or fatigue behavior of materials[33] as well as in following crack trajectory and study of toughening mechanisms after the experiment. The good match in the slope of the unloading curve of the first loading cycle and the loading part of the second loading cycle shows that the beam undergoes pure elastic deformation before final fracture. The feature of stable crack growth also allows generation of real cracks from the FIB machined notch tip by careful loading so that the effect of a finite notch root radius, if any, can be discounted for. The almost constant value of K_{IC} obtained at two different *a*/*w* ratios, one at the onset of the crack from the notch tip (0.89 MPa $m^{1/2}$) [Fig. 2(b-I)] and the other for the extension of the crack tip [Fig. 2(b-II)] (0.81 MPa $m^{1/2}$), coincides with the absence of an *R*-curve behavior. The two values also demonstrate that there is no undesirable effect of a notch root radius. This also reveals that FIB induced damage around the notch tip does not significantly alter the K_{IC} measurements, since crack growth of over 500 nm clearly surpasses the expected length scale of the damage zone (which is around 10–15 nm) but the observed fracture toughness is not affected at all. Issues associated with possibility of edge cracking and plasticity at the clamped ends have already been addressed.[29] The primary drawback currently for this geometry is the lack of analytical formulation for K_I since K_I does not follow a monotonically linear relationship with increasing *a*/*w* ratio in this case.[29] Hence each test requires an FEM simulation to be run to extract the stress intensity factor. Also, the notch requires to be cut from the side, and hence this geometry cannot be tested in the bulk but only at the sample edge. Another disadvantage is the difficulty encountered with respect to positioning the crack plane along a particular microstructural feature, since mode I loading in this geometry requires the crack plane to be at the exact center of the beam. As a consequence, it is more challenging to test heterostructures in this geometry, especially specific interfaces, compared to single cantilever bending. Residual stresses are an issue that clamped beam structures need to account for as they are in contiguous contact with the rest of the sample. The value of residual stress must be taken into account in the FEM simulation, which in turn requires independent measurements, e.g., by x-ray diffraction,[42] wafer curvature,[43] micro-Raman,[44] static deflection of microcantilevers,[45] and pillar micromachining combined with nanoindentation.[46] When appropriately accounted for, this can also be an advantage because this is one geometry where the effect of residual stress will be reflected in the fracture process, while in other test

https://doi.org/10.1557/jmr.2015.2 Published online by Cambridge University Press

methods, the samples are free from such stresses and the crack is no more under the influence of it.

For Si(100), a K_{IC} of 0.81 ± 0.1 was found from this geometry.

C. DCB

The DCB by compression using a flat punch [Fig. 2(c)] is one of the very recent geometries for fracture toughness testing, first demonstrated on CrN based hard, brittle coatings.[27] The conventional DCB has been the geometry of choice at the macroscale for many materials and is known to be stable under displacement control. Several modifications like the tapered DCB and wedge loaded DCB have followed to improve the stability of this geometry.[47–49] At the microscale, Liu et al.[27] demonstrated that a compression loading from the top can be translated into a tensile loading on the crack plane when some critical aspect ratios with respect to beam dimensions are maintained. In the present work on Si, this geometry did not support any stable crack growth, and all the specimens fractured catastrophically after the initial crack opening. This could be possibly due to the compliant nature of the indenter testing system, which has been explained already in Sec. I. A large part of the energy during compression of the double cantilever geometry is stored in the load frame of the indenter. This stored energy is released spontaneously as the crack propagates, rendering the beam unstable and causing catastrophic failure. This is not an issue as much for single cantilever and clamped beam bending experiments because the cantilevers in those cases are much more compliant themselves. It might be possible to arrest crack growth by using tapered beams and longer cantilever arms but this was not explored in the present work. In the formulation proposed by Liu et al.,[27] this geometry completely avoids the measurement of the crack length and only requires fracture load as the input to calculate the K_{IC}. This is the reason that a K_{IC} measurement was possible despite the absence of any stable crack growth. In the present work, a value of 0.08 was assumed for the friction coefficient μ between the Si wafer and the diamond tip[50] for the calculation of the stress intensity factor. Also, in Liu et al.'s tests on CrN coatings,[27] plastic deformation of the supporting pillars was avoided by maintaining a fixed ratio between the cantilever arm lengths and width of the beam. These bring about more restrictions on beam dimensions compared to the single cantilever and clamped beam geometries. The main advantage of using a flat punch in compression instead of a wedge to open the two cantilevers (Fig. 4) is to avoid friction from playing a major role although contact stresses do play a role in both cases. The rubbing action produced by the wedge tip in contact with the side walls of the two cantilevers will require modeling, complicating the analysis further. Also, the wedge has to be exactly centered between the two cantilever arms to give rise to mode I loading. The positioning of the flat punch is not that critical. But unlike in a conventional pillar compression test, it is important to ensure that the flat punch surface touches the two cantilever heads simultaneously, i.e., the surface of the flat punch and the two cantilever heads need to be exactly parallel to each other. Any misalignment creates an asymmetry in the bending moment produced by the two cantilevers and hence cannot produce mode I loading. The symmetry of the crack plane with respect to the two cantilever arms is also crucial in this geometry, and minor, inadvertent beam shifts during FIB milling can pose a problem. Hence it is challenging to position the notch plane along a particular microstructural feature (e.g., interface type) in this geometry. The type of materials that can be tested using this geometry are restricted to brittle systems whose cleavage plane or columnar boundaries are oriented in the direction of the initial crack.

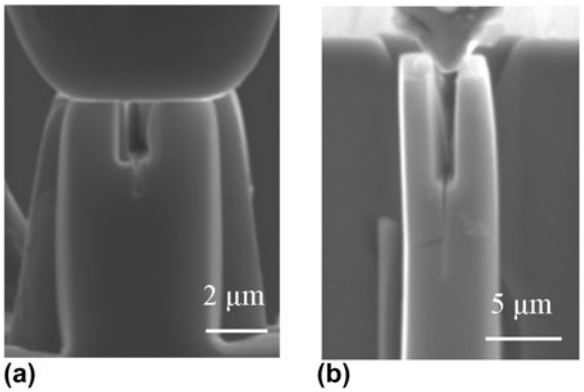


FIG. 4. DCB initiated by (a) flat punch compression and (b) wedge opening.

For Si(100), a K_{IC} of 0.89 ± 0.12 was found from this geometry.

D. Pillar splitting

Pillar splitting [Fig. 2(d)] is a novel geometry proposed by Sebastiani et al.[28] based on radial cracks produced by sharp indenters on brittle materials. This test geometry requires machining pillars with aspect ratios close to 1 and loading them at the center using a Berkovich/cube corner to produce radial cracks which split open the pillars into three equal parts. The geometry is simple, elegant, and easy to test. The formulation makes K_I independent of crack length which is the main advantage of this geometry though it does not account for the ratio of crack length to pillar radius. The constant γ that appears in Eq. (3) needs to be calculated for a variety of materials with different *E*/*H* ratios and is presently done using an FEM formulation which assumes the material to be homogeneous, linear elastic, and isotropic.[28] The disadvantage is that γ is very sensitive to the materials' *E*/*H*

https://doi.org/10.1557/jmr.2015.2 Published online by Cambridge University Press

ratio, whose value must be accurately known by other independent means. Sebastiani calculated a γ value of 0.305 (Ref. 32) assuming a Berkovich tip and isotropic elastic properties in the FEM simulations for K_{IC} calculations, while in the present work, a cube corner was used and a single crystal with anisotropic elastic properties was tested. Despite not accounting for these differences, the value of K_{IC} obtained by pillar splitting here is similar to the ones obtained from the other three geometries, with a difference of less than 10% compared to the average value. While the testing of homogeneous isotropic materials and transversely isotropic materials is straightforward, sufficient care needs to be taken in testing highly anisotropic materials, since crack propagation is not expected to be symmetric and to the same depth in all three directions. The crack lengths in all three directions in the present work were seen to be nearly equal, which would mean that Si is less sensitive to variations in the cracking direction as long as the indentation plane is kept constant. Ebrahimi and Kalwani showed that the measurements of indentation fracture toughness gave a constant value for a given plane, within the error bars of the measurement.[7] Being very close to an indentation test method and the associated complex tri-axial stress field underneath, it is difficult to maintain mode I conditions while testing heterogeneous materials. Also, this test is valid for materials which are brittle enough to produce radial cracks, and not undergo substantial plastic deformation or phase transformations during indentation. Phase transformation in Si is usually only observed during unloading as a pop-out, during nanoindentation with a pyramidal tip. In the pillar splitting test, the pillar cracks catastrophically to such a large extent that not sufficient data points are recorded in the unloading curve due to the uncontrolled movement of the low-stiffness indenter. In any case, Pharr[51] demonstrated that below threshold loads of 5–20 mN for a Berkovich, no phase transformations could be detected in the nanoindentation unloading curves in the form of pop-outs. The fracture loads, in the present work, were lower than this threshold value. But care should be exercised when pop-in or pop-out signatures occur in the P–d curve without accompanying cracking.

For Si(100), a K_{IC} of 0.75 $\pm$ 0.16 was found from this geometry.

E. Comparison of the four test geometries and further guidelines for microscale fracture toughness testing

The fracture toughness of Si(100) as obtained from the four different test configurations is given in Table I. These results are reported from five valid tests in each geometry. It is clear from Table I that the K_{IC} obtained with less than 15% variation between different test methods is independent of the test geometry. The standard deviation within a given test method is less than 16%, indicating a good reproducibility of the material's fracture toughness for each geometry. Although FIB has become the most commonly used tool to machine samples in the small-scale mechanics community, there arise issues regarding the extent of ion implantation and damage that FIB causes in the material and whether that can alter the overall deformation and fracture mechanism. But as shown in the present work, the K_{IC} of 0.75–0.89 MPa $m^{1/2}$ obtained from the FIB micromachined specimen is the same as the broadly accepted value of K_{IC} for single crystalline Si(100).[11] This should be sufficient evidence that there is no effect of redeposition and Ga^+ ion implantation damage, at least for microscale Si samples. This value is also proof that a notch root radius kept below 200 nm behaves like a real crack and does not lead to overestimation of fracture loads. In fact, this has already been shown by Wurster et al.[37] and Iqbal et al.[38]

Table II summarizes the above four fracture toughness test geometries listing the advantages and limitations of each, to serve as a guideline for future users. Besides specific geometry issues highlighted in this table, there are other generic issues that crop up during small scale testing dealing with fracture. The almost constant value of K_{IC} found for Si(100) from the four completely different geometries in the present work (Table I) suggests that the other reported values of K_{IC} in the literature both at the bulk and small-scale require a re-look. Fracture toughness determination requires both exactness in estimation and minimization of error in terms of scatter in the data. Keeping up with standard geometries becomes nearly impossible at the small-scale, especially in testing thin wafers like that of Si. The reasons for under or overestimation of K_{IC} are a consequence of the nonstandard geometry of the tests and the accompanying method of precracking or notching the specimens. As has already been stressed, the first and foremost condition in the application of fracture mechanics in the linear elastic regime is to maintain sample dimensions which are much larger than the plastic zone size of the sample. The other requirement of a valid K_{IC} test is that of maintaining plane strain conditions in test geometries that have a starter notch. In the present work, both the conditions are satisfied. There is sufficient evidence that Si can exhibit room temperature brittle to ductile transition and plasticity when the sample dimensions are scaled down to the nanoregime (below ~500 nm) due to either pressure induced phase transitions or dislocation activated amorphization.[52–54] For less brittle systems, one has to be more careful because the critical sample dimensions required to avoid plasticity will be higher. Mode I conditions need to be strictly adhered to in K_{IC} measurements and this is only possible in the given geometries if the material is isotropic, homogeneous, or in case of heterogeneous, anisotropic materials, if the

https://doi.org/10.1557/jmr.2015.2 Published online by Cambridge University Press

TABLE II. General guidelines for choosing a fracture toughness test geometry at the micrometer scale.

Test method	Input parameters (in addition to geometry)	Indenter type	In-situ required	Stable crack growth	Tolerance to misalignments	Contact and friction problems	Free of residual stress	Suitable for anisotropic materials	Suitable for interfaces	Ease of scaling	Success rate (successful tests/total tests)
Single cantilever bending	P_{max}, a	Wedge/Cone	×	×	✓	×	✓	✓	✓	✓	5/5
Clamped beam bending	P_{max}, a	Wedge/Cone	✓	✓	~	×	×	✓	✓	✓	5/6
Double cantilever bending	P_{max}, μ	Flat	✓	✓*	×	✓	✓	✓	~	×	5/10
Pillar splitting	P_{max}, μ, E, H	Cube/Berkovich	~	×	~	✓	✓	×	×	×	5/9

✓:Yes; ×:No; ~:Maybe

* Not observed in the present case possibly due to instrument compliance

notch is positioned along the microstructural plane with the lowest fracture toughness, as within this study. Any kinking or branching of the crack will bring about mixed mode fracture and render the test invalid. In such cases, analytical formulations cannot be used anymore and FEM simulations are required to determine the K_I and K_{II} components. In bulk testing, microscopic kinks are accommodated as long as the crack travels in a straight path macroscopically. In small-scale testing, this is not straightforward since the intrinsic microstructure being probed is of a similar magnitude as the sample size. Hence, most measurements report a K_C instead of a K_{IC}.

An additional source of error comes due to the precracking procedures used.[55,56] Notching by DRIE can induce chemical effects. Indentation and scratch with sharp indenters and AFM tips can cause residual stresses and leave behind remnant impressions while ion slicing and FIB milling can induce Ga^+ ion damage. All of these techniques of creating a precrack can affect the K_{IC} of the material. In one of the first reported results on fracture in Si, Chen and Leipold[6] used a Knoop indenter to produce indentation cracks on single crystal Si with varying *c*/*a* ratios. They found a K_{IC} of 1 MPa $m^{1/2}$ on an average but also created a flaw length dependence of K_{IC}. Though this was an attempt to use real cracks instead of notches in fracture toughness testing, it brings in issues of deformation and residual stresses beneath the indenter. Additionally, the variance in the shape and uniformity of the elliptical crack arising due to anisotropy in Si was not described in their results. Neither were any load–displacement curves shown for comparison. Using notches in place of precracks for fracture toughness studies has always been questioned due to the finite notch root radius that causes overloading of the specimen.[14] Work by Myers and Hillberry[57] on the effect of notch root radius on fracture toughness values of single crystalline Si using four point bend geometry shows that overestimation by more than ~30% occurs in cases where the notch radii are 80 μm and more. Notch toughness values of poly-Si reported in the literature vary between 1.4 and 4.5 MPa $m^{1/2}$ depending on the notch root radii, which varied from 0.23 to 1 μm.[58] In contrast, FIB machined notches (at lowest currents) have a notch root radius below ~50 nm and are sufficiently small to behave like ideal cracks as seen from previous studies.[37,38] In the context of using FIB to machine notches at 30 keV and currents of ≤10 pA, the Ga^+ ion implantation depth and resulting amorphous thin film formation are not expected to be more than 30 nm in a hard material like Si.[59] It is clear that the FIB damage does not affect the measured fracture toughness value since the clamped beam specimen gives the same fracture toughness value (within error bars) at the notch tip and the crack tip

https://doi.org/10.1557/jmr.2015.2 Published online by Cambridge University Press

[Fig. 2(b)] as also the pillar splitting tests with no prenotch. With the specimen here being 2 orders of magnitude larger in dimension than the damage zone, and the plastic zone size of 200 nm itself being an order of magnitude larger than the expected point defect cluster size ($\leq$10 nm), ion damage is not expected to alter the brittle fracture behavior of Si. Therefore, it can be conclusively stated that notching with a FIB at the lowest currents possible creates a notch in Si whose tip behaves very close to that of an ideal crack, thus enabling measurement of the true K_{IC}.

Another important aspect of fracture toughness testing which is often ignored is the role of statistics. For example, Kahn et al.[60] carried out K_{IC} measurements using sharp cracks produced by indentation on poly-Si MEMS chips (which also acted as the fracture device). Although their median K_{IC} value is very close to earlier reported values (1.1 MPa $m^{1/2}$), they report a wide scatter in their data ranging from 0.2 to 2.2 MPa $m^{1/2}$, with a low Weibull modulus. The explanation they offered is that indentation cracks differ substantially in length and orientation due to stochastic effects. Chasiotis et al.[61] carried out similar tests on poly-Si using indentation induced cracks and obtained a value of 1 MPa $m^{1/2}$, and surprisingly a much lower scatter of 0.1 MPa $m^{1/2}$. Unlike polycrystalline Si, single crystal Si wafers are homogeneous and of high purity and are expected to show a low scatter in the K_{IC} data. In the present work, each test geometry showed different success rates but in general, geometries 1 and 2 showed more than 80% success. Geometries 3 and 4 showed less than 55% success. The low success rate of geometry 4 was due to the rapid catastrophic fracture and destruction of the pillar that occurred during loading. Geometry 3 had additional issues like the sample fracturing across the cantilever arms. Individual differences will also arise depending on the familiarity of the investigator with respect to a given geometry. Table II shows the number of samples that were found acceptable among the total number of samples tested. It was ensured that five valid tests were used from each geometry type for reporting the K_{IC} results in Table I. Even with the small sampling size, the scatter is quite low, making the value of K_{IC} obtained, acceptable. This is counter-intuitive since a smaller sampling size usually leads to a larger scatter. However, the present study shows that an optimum number of careful experiments accounting for actual sample dimensions and controlled crack lengths can yield correct results.

IV. CONCLUSION

Numerous small-scale test configurations have been recently developed for miniaturized fracture toughness measurements including the single cantilever bending, clamped beam bending, double clamped beam bending, and pillar splitting methods. When making a choice for a particular test geometry, one must give careful consideration about getting the true K_{IC} of the material along with the ease, convenience, and suitability of the test for the given sample or device. The above described four geometries have been proven to be valid fracture toughness test geometries, giving an average fracture toughness of 0.80 MPa $m^{1/2}$ for Si (100). This shows that any differences that are observed by future users on testing other materials may only be due to the inability of some of these test methods to capture the multiple microstructural complexities in them. Each one has limitations in terms of alignment, friction effects, and versatility in testing different types of materials which has been discussed in detail. Independence from test geometry is important in the determination of the real material property at any given length scale, particularly in the context of fracture toughness.

ACKNOWLEDGMENTS

The authors would like to gratefully acknowledge Dr Marco Sebastiani, Roma Tre, Italy for providing the γ value for calculation of K_I in the pillar splitting experiment.

REFERENCES

1. G. Dehm, C. Motz, C. Scheu, H. Clemens, P.H. Maryhofer, and C. Mitterer: Mechanical size effects in miniaturized and bulk materials. *Adv. Eng. Mater.* **8**(11), 1033–1045 (2006).
2. O. Kraft, P.A. Gruber, R. Moenig, and D. Weygand: Plasticity in confined dimensions. *Annu. Rev. Mater. Res.* **40**, 293–317 (2010).
3. J.R. Greer and J.D. Hosson: Plasticity in small scale metallic systems: Intrinsic vs extrinsic size effect. *Prog. Mater. Sci.* **56**(6), 654–724 (2011).
4. A.H. Chokshi, A. Rosen, J. Karch, and H. Gleiter: On the validity of Hall-Petch relationship in nanocrystalline materials. *Scr. Metall.* **23**, 1679–1684 (1989).
5. C.E. Carlton and P.J. Ferreira: What is behind the inverse Hall-Petch effect in nanocrystalline materials? *Acta Mater.* **55**, 3749–3756 (2007).
6. C.P. Chen and M.H. Leipold: Fracture toughness of Si. *Am. Ceram. Soc. Bull.* **59**, 469–472 (1980).
7. F. Ebrahimi and L. Kalwani: Fracture anisotropy in silicon single crystal. *Mater. Sci. Eng., A* **268**, 116–126 (1999).
8. S. Sundararajan and B. Bhushan: Development of AFM based techniques to measure mechanical properties of nanoscale structures. *Sens. Actuators, A* **101**, 338–351 (2002).
9. T. Ando, X. Li, S. Nakao, T. Kasai, H. Tanaka, M. Shikida, and K. Sato: Fracture toughness measurement of thin film silicon. *Fatigue Fract. Eng. Mater. Struct.* **28**, 687–694 (2005).
10. M. Tanaka, K. Higashida, H. Nakashima, H. Takagi, and M. Fujiwara: Orientation dependence of fracture toughness measured by indentation methods and its relation to surface energy in single crystal silicon. *Int. J. Fract.* **139**, 383–394 (2006).

https://doi.org/10.1557/jmr.2015.2 Published online by Cambridge University Press

11. R.O. Ritchie: Failure of silicon: Crack formation and propagation. In *13th Workshop on Crystalline Solar Cell Materials and Processes*, Vail, Colorado, 2003.
12. ASTM E 1820-01: Standard test method for measurement of fracture toughness. In *Ann Book ASTM Std*, Vol. **03.01**, 2001, pp. 1–46.
13. A. Yawny, J. Malarria, E. Soukup, and M. Sade: Stage for in-situ mechanical loading experiments in a scanning electron microscope with a small chamber. *Rev. Sci. Instrum.* **68**, 1500154 (1997).
14. B.N. Jaya and M.Z. Alam: Small-scale mechanical testing of materials. *Curr. Sci.* **105**, 1073–1099 (2013).
15. J.E.P. Ipina and A.A. Yawny: In-situ observation of damage evolution and fracture toughness measurement by SEM. In *Damage Prognosis for Aerospace, Civil and Mechanical Systems*, edited by D. J. Inman, D. J. Farrar, V. Lopes, Jr, and V. Steffen Jr. (2005); pp. 61–73.
16. R. Podor, J. Ravaoux, and H. Brau: In-situ experiments in the scanning electron microscope chamber. In *Scanning Electron Microscopy*, edited by V. Kazmiruk. (InTech, 2012); pp. 32–54.
17. B.N. Jaya, S. Bhowmick, S.A. S Asif, O.L. Warren and V. Jayaram: Optimisation of clamped beam geometry for fracture toughness testing of micron-scale samples. *Philos* (2015, in press). DOI.10.1080/14786435.2015.1010623.
18. W.C. Oliver and G.M. Pharr: An improved technique for determining hardness and elastic modulus using load and displacement sensing indentation experiments. *J. Mater. Res.* **7**, 1564–1583 (1992).
19. K.J.V. Vliet, L. Prchlik, and J.F. Smith: Direct measurement of indentation frame compliance. *J. Mater. Res.* **19**, 325–331 (2004).
20. S.A.S. Asif, K.J. Wahl, and R.J. Colton: Nanoindentation and contact stiffness measurement suing force modulation with a capacitive load-displacement transducer. *Rev. Sci. Instrum.* **70**, 2408–2413 (1999).
21. D. Kupka: Fracture experiments of single grain boundaries in ductile metals. PhD Thesis, Helmholtz-Zentrum Geesthacht, Germany, 2013.
22. E. Huerta, J.E. Corona, A.I. Oliva, F. Aviles, J. Gonzalez-Hernandez: Universal testing machine for mechanical properties of thin materials. *Rev. Mex. Fis.* **56**(4), 317–322 (2010).
23. A.C. Fischer-Cripps: *Nanoindentation*, 2nd ed. (Springer, New York, NY, 2004).
24. C.M. Peret and J.M. Rodrigues: Stability of crack propagation during bending tests on brittle materials. *Ceramica* **54**, 382–387 (2008).
25. K. Matoy, H. Schoenherr, T. Detzel, R. Pippan, C. Motz, and G. Dehm: A comparative microcantilever study of the mechanical behavior of silicon based passivation films. *Thin Solid Films* **518**, 247–256 (2009).
26. B.N. Jaya, V. Jayaram, and S.K. Biswas: A new method for fracture toughness determination of graded (Pt, Ni)Al bond coats by microbeam bend tests. *Philos. Mag.* **92**, 3326–3345 (2012). Special Issue: Nano-mechanical testing in materials research and development III.
27. S. Liu, J.M. Wheeler, P.R. Howie, X.T. Zeng, J. Michler, and W.J. Clegg: Measuring the fracture resistance of hard coatings. *Appl. Phys. Lett.* **102**, 1719071–1719074 (2013).
28. M. Sebastiani, K.E. Johanns, E.G. Herbert, F. Carasitti, and G. M Pharr: A novel pillar indentation splitting test for measuring fracture toughness of thin ceramic coatings. *Philos. Mag.* (2014). DOI: 10.1080/14786435.2014.913110.
29. B.N. Jaya and V. Jayaram: Crack stability in edge notched clamped beam specimen: Modeling and experiments. *Int. J. Fract.* **188**, 213–228 (2014).
30. M.A. Hopcroft, W.D. Nix, and T.W. Kenny: What is the Young's modulus of Si? *J. Microelectromech. Syst.* **19**, 229–238 (2010).
31. S. Timoshenko and J.N. Goodier: *Theory of Elasticity*, 2nd ed. (McGraw-Hill, New York, NY, 1951).
32. M. Sebastiani: Private communication, 2014.
33. H. Li and J.J. Vlassak: Determining the elastic modulus and hardness of an ultra-thin film on a substrate using nanoindentation. *J. Mater. Res.* **24**, 1114–1126 (2009).
34. D. Di Maio and S.G. Roberts: Measuring fracture toughness of coatings using focused-ion-beam-machined microbeams. *J. Mater. Res.* **20**, 299–302 (2005).
35. K. Takashima and Y. Higo: Fatigue and fracture of a Ni-P amorphous alloy thin film on the micrometer scale. *Fatigue Fract. Eng. Mater. Struct.* **28**, 703–710 (2005).
36. T.P. Halford, D. Rudinal, K. Takashima, and Y. Higo: The effect of sample preparation upon the fracture toughness of microsized TiAl. *Key Eng. Mater.* **297–300**, 2416–2422 (2005).
37. S. Wurster, C. Motz, and R. Pippan: Characterisation of fracture toughness of micron-sized tungsten single crystal notched specimens. *Philos. Mag.* **92**, 1803–1825 (2012).
38. F. Iqbal, J. Ast, M. Goeken, and K. Durst: In-situ microcantilever tests to study fracture properties of NiAl single crystals. *Acta Mater.* **60**, 1193–1200 (2012).
39. D.E.J. Armstrong, A.J. Wilkinson, and S.G. Roberts: Micro-mechanical measurements of fracture toughness of bismuth embrittled copper grain boundaries. *Philos. Mag. Lett.* **91**(6), 394–400 (2011).
40. M. Mueller: Microscopic chevron-notch fracture test of alumina reinforcements. Nanobruecken (2014).
41. F. Iqbal: Fracture mechanisms of γ-TiAl alloys investigated by in-situ experiments in a scanning electron and atomic force microscope. PhD Thesis, Universität Erlangen-Nürnberg, Erlangen, Germany, 2012.
42. I.C. Noyen and J.B. Cohen: *Residual Stress Measurement by Diffraction and Interpretation* (Springer-Verlag, New York, 1987).
43. A. Brenner and S. Senderoff: Calculation of stress in electrodeposits from the curvature of a plated strip. *J. Res. Natl. Bur. Stand.* **42**, 105–123 (1949).
44. J.W. Ager, III and M.D. Drory: Quantitative measurement of residual biaxial stress by Raman spectroscopy in diamond grown on a Ti alloy by chemical vapor deposition. *Phys. Rev. B.* **48**, 2601–2607 (1993).
45. W. Fang and J. Wickert: Determining mean and gradient residual stresses in thin films using micromachined cantilevers. *J. Micromech. Microeng.* **6**, 301–309 (1996).
46. M. Sebastiani, E. Bemporad, F. Carasitti, and N. Schwarzer: Residual stress measurement at the micrometer scale: Focused ion beam milling and nanoindentation testing. *Philos. Mag.* **91**, 1121–1136 (2011).
47. W. Beres, A.K. Koul, and R. Thamburaj: A tapered double cantilever beam specimen designed for constant K-testing at elevated temperatures. *J. Test. Eval.* **25**, 536–542 (1997).
48. E.N. Brown: Use of the tapered double-cantilever beam geometry for fracture toughness measurements and its application to the quantification of self-healing. *J. Strain Anal. Eng. Des.* **46**, 167–186 (2010).
49. Y. Qiao: PhD Thesis, MIT, 2002.
50. H.H. Gatzen and M. Beck: Investigations on the friction force anisotropy of the silicon lattice. *Wear* **254**, 1122–1126 (2003).
51. G.M. Pharr: The anomalous behavior of silicon during nanoindentation. *Mater. Res. Soc. Symp. Proc.* **239**, 301–312 (1992).
52. W.W. Gerberich, D.D. Stauffer, A.R. Beaber, and N.I. Tymiak: A brittleness transition in silicon due to scale. *J. Mater. Res.* **27**, 552–567 (2012).

https://doi.org/10.1557/jmr.2015.2 Published online by Cambridge University Press

53. Z. Han, K. Zheng, Y.F. Zhang, Z. Zhang, and Z.L. Wang: Low temperature in-situ large strain plasticity of silicon nanowires. *Adv. Mater.* **19**, 2112–2118 (2007).
54. F. Oestlund, K.R. Malyska, K. Leifer, L.M. Hale, Y. Tang, R. Ballarini, W.W. Gerberich, and J. Michler: Brittle to ductile transition in uniaxially compression of silicon pillars at room temperature. *Adv. Funct. Mater.* **19**, 2439–2444 (2009).
55. P. Gludovatz, S. Wuster, A. Hoffmann, and R. Pippan: A study into the crack propagation resistance of pure tungsten. *Eng. Fract. Mech.* **100**, 76–85 (2013).
56. T. Tsuchiya, J. Sakata, and Y. Taga: Tensile strength and fracture toughness of surface micromachined polycrystalline silicon thin films prepared under various conditions. *MRS Symp. Proc.* **505**, 285–290 (1997).
57. R.J. Myers and B.M. Hillberry: Effect of notch root radius on the fracture behavior of monocrystalline silicon. In *Proceedings, 4th International Conference on Fracture, Waterloo, Canada*, Vol. **3**, 1001–1005 (1977).
58. W.N. Sharpe, B. Yuan, and R.L. Edwards: Fracture tests of polysilicon film. *MRS Symp. Proc.* **505**, 51–56 (1997).
59. S. Rubanov and P.R. Munroe: FIB induced damage in silicon. *J. Microsc.* **24**, 213–221 (2004).
60. H. Kahn, N. Tayebi, R. Ballarini, R.L. Mullen, and A. H. Heuer: Fracture toughness of polysilicon MEMS devices. *Sens. Actuators, A* **82**, 274–280 (2000).
61. I. Chasiotis, S.W. Cho, and K. Jonnalagadda: Fracture toughness and subcritical crack growth in polycrystalline silicon. *J. Appl. Mech.* **73**, 714–722 (2005).

https://doi.org/10.1557/jmr.2015.2 Published online by Cambridge University Press